ADVANCED
QUANTUM
TECHNOLOGIES

Photonic Jet Writing of Quantum Dots Self-Aligned to Dielectric Microspheres

Andrea Ristori, Travis Hamilton, Dimosthenis Toliopoulos, Marco Felici, Giorgio Pettinari, Stefano Sanguinetti, Massimo Gurioli, Hooman Mohseni, and Francesco Biccari*

Owing to their ability to generate non-classical light states, quantum dots (QDs) are very promising candidates for the large-scale implementation of quantum information technologies. However, the high photon collection efficiency demanded by these technologies may be impossible to reach for "standalone" semiconductor QDs, embedded in a high-refractive index medium. In this work a novel laser writing technique is presented, enabling the direct fabrication of a QD self-aligned—with a precision of ± 30 nm—to a dielectric microsphere. The presence of the microsphere leads to an enhancement of the QD luminescence collection by a factor 7.3 ± 0.7 when an objective with 0.7 numerical aperture is employed. This technique exploits the possibility of breaking the N—H bonds in $GaAs_{1-x}N_x$:H by a laser light, obtaining a lower-bandgap material, $GaAs_{1-x}N_x$. The microsphere, deposited on top of a $GaAs_{1-x}N_x$:H/GaAs quantum well, is used to generate a photonic nanojet, which removes hydrogen exactly below the microsphere, creating a $GaAs_{1-x}N_x$ QD at a predefined distance from the sample surface. Second-order autocorrelation measurements confirm the ability of the QDs obtained with this technique to emit single photons.

1. Introduction

The interest in semiconductor quantum dots (QDs) has increased in the last 2 decades, when it became clear that they could become a fundamental building block for the development of quantum information technologies[1] (e.g., quantum computers and quantum cryptography), thanks to their ability to act

as a source of non-classical light states. In particular, epitaxially grown semiconductor QDs, as opposed to other quantum emitters such as single atoms or colloidal QDs, present the advantage of being natively embedded within a solid-state matrix, which fixes their position and makes them uniquely suited for the integration in electronic devices.[2]

However, the presence of a solid-state environment also has a drawback: since the refractive index (n) of the bulk material surrounding the QDs is typically as high as 3.5, total internal reflection limits the extracted luminescence power from a planar sample into air to a very small fraction of the emitted power (0.06–2.1%, depending on the dipole axis orientation).[3] Moreover, the numerical aperture (NA) of the collecting optics limits the collected luminescence even further. Therefore, even if the QD emits exactly one photon during each excitation cycle, the system is not really deterministic: the photon counts per second (N) will, indeed, follow a binomial distribution, $f(N; N_0, p)$, where N_0 is the number of excitations per second and p is the photon collection probability (Fano factor $= 1 - p \approx 1$). This is undesirable in most applications, such as quantum cryptography[4] and quantum computing,[5] where higher collection efficiencies give rise to faster and more reliable operations.

A. Ristori, Prof. M. Gurioli, Dr. F. Biccari
Department of Physics and Astronomy
University of Florence
Via G. Sansone 1, Sesto Fiorentino, Florence I-50019, Italy
E-mail: francesco.biccari@unifi.it

A. Ristori, Dr. F. Biccari
European Laboratory for Non-Linear Spectroscopy (LENS)
University of Florence
Via N. Carrara 1, Sesto Fiorentino, Florence I-50019, Italy

Dr. T. Hamilton, Prof. H. Mohseni
Bio-Inspired Sensors and Optoelectronics Laboratory
Northwestern University
2145 Sheridan Rd, Evanston, IL 60208, USA

Dr. D. Toliopoulos, Prof. S. Sanguinetti
Department of Material Science
University of Milano-Bicocca
Via Cozzi 55, Milano I-20125, Italy

Prof. M. Felici
Department of Physics
Sapienza-University of Rome
Piazzale Aldo Moro 5, Roma I-00185, Italy

Dr. G. Pettinari
Institute for Photonics and Nanotechnologies (CNR-IFN)
National Research Council
Via Cineto Romano 42, Roma I-00156, Italy

**ADVANCED
SCIENCE NEWS**

www.advancedsciencenews.com

**ADVANCED
QUANTUM
TECHNOLOGIES**

www.advquantumtech.com

To solve these issues, several solutions have been proposed throughout the years. Among these solutions,[6] the ones that give the best results require a hardly achievable spatial and spectral coupling between the QDs and an external resonator, for example microcavities,[7] photonic crystal (PhC) cavities alone[8] or coupled with waveguides,[9] and circular Bragg gratings.[10] Thanks to the development of broadband alternatives such as microspheres,[11] 3D printed microlenses,[12–14] nanowires,[15] nanorings alone[16] or combined with other broadband solutions,[17] and photonic trumpets (with 95% out-coupling record efficiency),[18] the spectral coupling problem has been partially solved, but these devices still require an accurate positioning of the QDs. Moreover, all these techniques require complex nano-fabrications and/or nano-manipulations, strongly limiting the scalability of these solutions, which are also irreversible, expensive, and subject to possible failure in the nanofabrication process. A second kind of solutions, albeit characterized by generally lower performances, is largely exempt from these drawbacks, since the desired collection efficiency enhancement is obtained by placing a millimeter lens, a spherical cap, called solid immersion lens (SIL), on the sample, on top of the emitters.[19] It is a spectrally and spatially tolerant tool, which can be easily and reversibly placed on the sample. Its main drawback is represented by the relatively small enhancement a SIL can achieve: indeed, it can only increase the NA of the system by a factor equals to its refractive index, n_L, and thus its collection enhancement is about n_L^2.[20] However, a SIL can also be combined with other broadband solutions to further increase the collection enhancement,[17,21] yet reintroducing the problem of realizing complex nano-fabrications and/or nano-manipulations. Finally, other drawbacks of the SILs include their bulky nature (mm-size), which is not ideal for many applications, and their sensitivity to the air-gap which can arise between them and the sample surface.[20]

In this work, we propose an innovative method for the hybrid integration of a dielectric antenna on top of a buried QD, which gives a broadband, reversible, and low-cost solution to the light collection problem, by exploiting dielectric microspheres for creating self-aligned QDs. Indeed, it is known that the presence of a microsphere on top of an emitter helps the collection process[11,22] due to an increase in the NA of the system, and lately this has been verified also for QDs.[23] The main drawback of this approach is the requirement of a precise positioning of the microsphere on top of the QD, with an accuracy one order of magnitude smaller than the microsphere size itself; plus, a QD position even slightly off-axis leads the luminescence to be directed at a non-normal angle with respect to the sample surface.[23] We circumvented this issue by exploiting the microspheres not only for the collection process, but also for the QD fabrication: by harnessing the properties of hydrogenated $GaAs_{1-x}N_x$ in conjunction with the so called photonic nanojets—one of the most striking features characterizing the microspheres[24–28]—our novel technique allows to "laser write" $GaAs_{1-x}N_x$ QDs exactly below the microspheres, "self-aligned" with their central axis.

$GaAs_{1-x}N_x$ is the most representative case of dilute nitride semiconductors, that is, III–V semiconductor alloys with a small percentage (typically less than 5%) of N in the V-group sublattice.[29] The introduction of N in III–V alloys strongly perturbs the conduction band structure, reducing the bandgap. For instance, with a N percentage of ≈ 1%, the bandgap of $GaAs_{0.99}N_{0.01}$ is 1.3 eV at 10 K,[30] about 200 meV lower than the GaAs bandgap value. The introduction of hydrogen into $GaAs_{1-x}N_x$ leads to the formation of two stable complexes (up until 315 and 235 °C, respectively), N-2H and N-2H-H, which completely wipe out all nitrogen effects, gradually restoring the bandgap, effective mass, spin properties, refractive index, lattice constant, and ordering of the N-free material.[29,31] All these effects can be controlled by regulating the H concentration in the material.

2. QD Fabrication Technique

The sample used in this work is a fully hydrogenated $GaAs_{1-x}N_x$:H/GaAs ($x = 0.011$) QW grown on top of an (Al,Ga)As sacrificial layer deposited on a GaAs substrate. The sacrificial layer is then removed in limited areas of the sample to suspend the QW from the substrate. The suspended membranes were realized by patterning the sample surface with circular apertures and removing the (Al,Ga)As sacrificial layer by a wet etch, as shown in **Figure 1**a (see Section 5 for further details). The idea is that in the future we could fabricate a PhC cavity on our suspended membranes, in order to further enhance the QD emission or, in general, to better control the properties of the emitted light.[32] The circular suspended membranes were also used to easily identify the QDs on the sample, as well as to increase the back reflection of the QD emission, thanks to the presence of an additional GaAs/air interface underneath the QD. The membrane thickness (166 nm) was chosen to exclude the presence of any slab waveguide modes of order higher than the fundamental ones (TE_0 and TM_0) in the wavelength range of interest (about 900 nm). Following this procedure, dielectric microspheres were air-sprayed on the sample surface, as sketched in Figure 1c. A SEM image of the surface of the sample is reported in Figure 1b, where the deposited microspheres are clearly visible; the inset displays a magnification of a single microsphere, located on top of a suspended membrane. The microspheres are made of SiO_2 and have a nominal diameter of 2 μm (see Section 5 for further details). Such microspheres have been reported to give rise to narrow photonic jets in similar samples.[23]

The QDs were obtained by exploiting the possibility to break the N−H bonds by illuminating the sample with a laser light of proper wavelength (500 nm < λ < 830 nm),[33] following our previous work on QD fabrication by a scanning near-field optical microscopy equipped with a tapered fiber (SNOM tip).[34] In particular, we controlled the hydrogen removal process in the $GaAs_{1-x}N_x$:H/GaAs QW by using photonic nanojets. A photonic nanojet is a highly intense light beam characterized by a sub-wavelength spatial extension, obtained below a microsphere illuminated with a plane wave of proper λ.[26] Illuminating a microsphere, we were able to remove hydrogen in a nanometric region of the QW, creating a $GaAs_{1-x}N_x$ nanocrystal surrounded by $GaAs_{1-x}N_x$:H in the lateral direction and GaAs in the vertical direction, obtaining the 3D energy confinement necessary to define a QD (see Figure 1d).

To predict the photonic nanojet properties in our sample, we performed 2D simulations with the finite-difference time-domain (FDTD) method, using the FDTD 3D electromagnetic
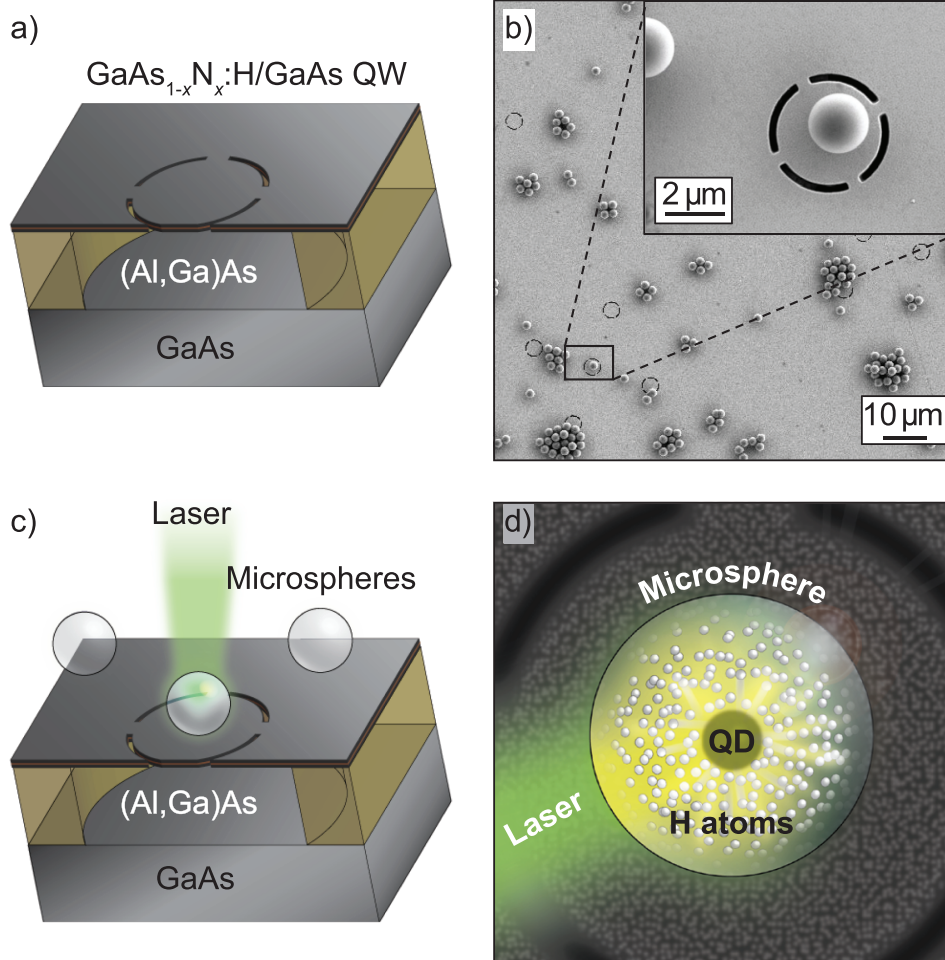
Figure 1. a) Sketch of the sample. b) SEM image of the sample with microspheres on top. In the inset: magnification of a single microsphere on top of a suspended membrane. c) Schematic example of the microspheres deposited on top of the sample and representation of the GaAs$_{1-x}$N$_x$ QD fabrication process, based on illuminating a microsphere with a laser light (see main text). d) Artistic representation (view from top) of the QD formation process: the photonic jet formed during illumination breaks the N−H bonds present in the GaAs$_{1-x}$N$_x$:H QW, leaving a GaAs$_{1-x}$N$_x$ QD below the microsphere.

simulator from Lumerical Inc (version 2020R2.4). We simulated the propagation of a plane wave with $\lambda = 532$ nm over our sample, wherein a microsphere was placed on top of a membrane. The selected value of λ should result in a proper photonic jet for the diameter of our microspheres, characterized by a subwavelength profile width. The results of the simulation are shown in **Figure 2**, which displays the magnitude of the Poynting vector in false colors. As we can see, a nanometric beam of light is indeed created below the microsphere, with an extension of about 266 nm at its FWHM, $\approx \lambda/2$ (see the ×3 magnification and its profile in the insets).

The GaAs$_{1-x}$N$_x$ QDs obtained in this work were created at room temperature and in air, by using a diode-pumped solid state laser at 532 nm with different powers, ranging from 58 to 70 mW in 4 mW steps. We want to point out that the absolute value of the fabrication power depends on the optical system, wavelength, microsphere material and diameter, sample characteristics, etc. Therefore, this power must be calibrated on a sample-to-sample basis, by carrying out a few tests for each QD fabrication run.

3. Results and Discussion

The QDs were characterized by their photoluminescence (PL) (see Section 5 for further details) at low temperature ($T = 10$ K). Indeed, the carrier confinement in these QDs is not very high and their PL can be observed up to about 100 K.[31,32] This value varies on the material quality and composition: the QDs fabricated in our material, containing a typical value of 1% of nitrogen, show a barrier of 245 meV in the conduction band and of about 7 meV in the valence band.[31,34]

The low-temperature ($T = 10$ K) PL spectra of a series of QDs, fabricated with the same exposure time (1 s) and with different fabrication power, are reported in **Figure 3**. Clear sharp emissions are observed (identification of the emission lines is reported in the Supporting Information). The PL spectrum of the QW before hydrogenation is also reported for comparison, as the QW emission energy (about 1.30 eV in our case) represents the lower limit for the QD emission energy. Indeed, if hydrogen is removed from an area large enough to make the quantum confinement effect negligible in the horizontal direction, the fabricated QDs
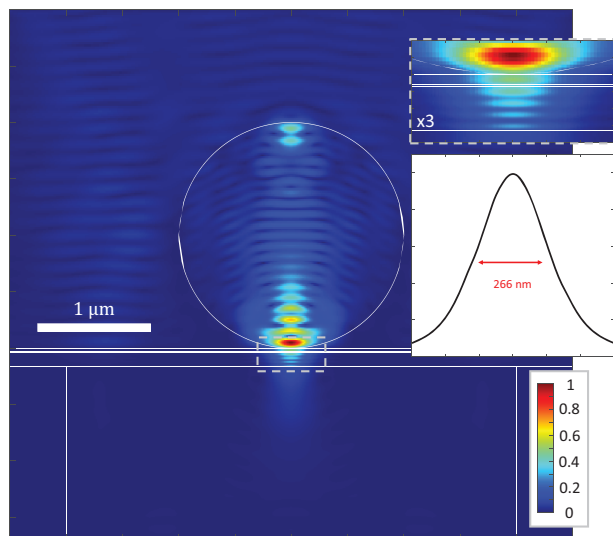
**ADVANCED
SCIENCE NEWS**

www.advancedsciencenews.com

**ADVANCED
QUANTUM
TECHNOLOGIES**

www.advquantumtech.com

Figure 2. Poynting vector magnitude (normalized to the maximum) obtained by an FDTD simulation of our sample with one microsphere on top of a suspended GaAs$_{1-x}$N$_x$:H/GaAs QW, under illumination with a plane wave ($\lambda = 532$ nm). The white lines represent the contour of our sample and the microsphere. The insets show a ×3 magnification of the photonic jet area and its profile.
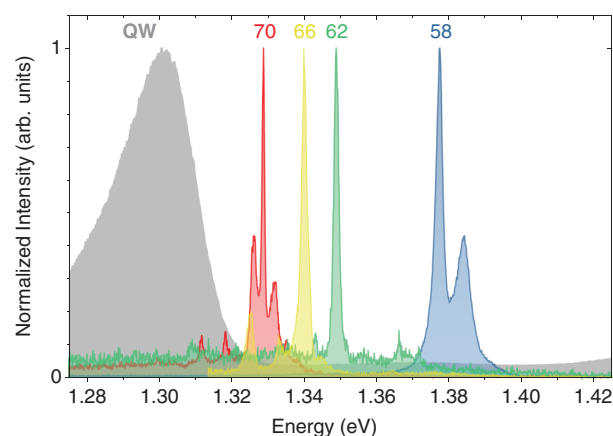

Figure 3. PL spectra, measured at 10 K and with an CW excitation power of $P_{exc} = 300$ nW, of four different QDs fabricated at different fabrication powers, distinguished by colors, and with the same exposure time (1 s). The fabrication powers, in units of mW, are provided as labels. The shaded spectrum correspond to the PL spectrum of the GaAs$_{1-x}$N$_x$/GaAs QW before hydrogenation.

approach the QW's behavior. The upper limit is reached instead when the fabrication power creates a dot so small that its first excitonic energy level is comparable, within few kT, to the barrier excitonic level. However, it is impossible to directly observe this limit by optical measurements, since the smaller the dot, the lower the PL emitted by the QD.

The intensity of the main line of our QDs shows a large range of variation. An upper limit for the overall efficiency of our system can be given using the tabulated data for all the elements of our setup (see Supporting Information). According to the reported data, the efficiency can be estimated to be about 4% at 930 nm. Using this value, we can estimate the lower limit of photons per

second, corresponding to the integral over the emission line, impinging on the first lens of the setup (brightness). At the saturation power of the QD emission line under investigation, under CW excitation, and in presence of the microsphere, the brightness ranges between 0.2×10^6 and 5×10^6 s^{-1}. This large variation is likely mainly due to the different concentration of non-radiative defects in proximity of the QD. It is also interesting to note a trend of the luminosity with emission energy: the higher the emission energy, the smaller the dot, the lower the luminosity. This phenomenon is compatible with our hypothesis: due to the higher surface to volume ratio for smaller QDs, the influence of non-radiative defects surrounding the QD is larger.

The size of the QDs can be estimated, after reasonable assumptions,[34] by using the measured QD emission energy. According to the simple model developed in ref. [34], the QD diameters span the range between 10 and 6.8 nm, obtained with fabrication powers between 70 and 58 mW, respectively. While this determination of the QD sizes should only be taken as a rough estimate, the observation of pronounced lateral quantum confinement effects confirms that the diameter of the fabricated QDs must be at least of the order of the size of free exciton, which in GaAs$_{1-x}$N$_x$ is less than 10 nm.[29] This proves our ability to remove hydrogen from an area much smaller than the diffraction limit by employing photonic nanojets. It seems surprising that the QD diameter ($\approx$ 10 nm) is much smaller than the FWHM of the photonic jet ($\approx$ 250 nm) and that only one QD is formed within the jet. This can be explained as follows: while the wavelength and the excitation power determine the amount of broken N−H bonds, the temperature gradient and the exposure time determine the extent to which H diffuses, and therefore the diameter of the QD. The power profile of the photonic jet is Gaussian, and H is only removed from the central portion of the beam, where the power density is above a certain threshold. Outside of this region, which can be considerably narrower than the beam's FWHM, there is a much lower probability of forming QDs.

For each fabrication power we measured several (> 10) nominally identical QDs obtaining a spread of the central QD-emissions with a FWHM value of about 40 meV. This inhomogeneous broadening is related to many factors: fluctuations in the optical properties of the individual microspheres and of the sample surface give rise to variations in the photonic jet shape; since the H removal process has also a thermal component,[35] local variations in the heat dissipation efficiency of the material (due, for example, to the positioning of the microsphere with respect to the circular apertures opened in the suspended membranes, see Figure 1b) influence the H removal; finally, fluctuations of thickness, and N and H concentrations in the starting QW put a lower limit for the inhomogeneous broadening of the QDs. Considering that the QW emission shows a 30 meV broadening (see Figure 3), this factor is likely to predominate over the others, leading to the conclusion that an improvement of the quality of the QW would be crucial to significantly lower the QD inhomogeneous broadening.

It is interesting to calculate the minimum inhomogeneous broadening of an ensemble of nominally identical QDs. Assuming a perfectly flat QW and a perfect fabrication process, the minimum inhomogeneous broadening is due to N concentration fluctuations. Given a generic volume V, since the fluctuations

**ADVANCED
SCIENCE NEWS**

www.advancedsciencenews.com

**ADVANCED
QUANTUM
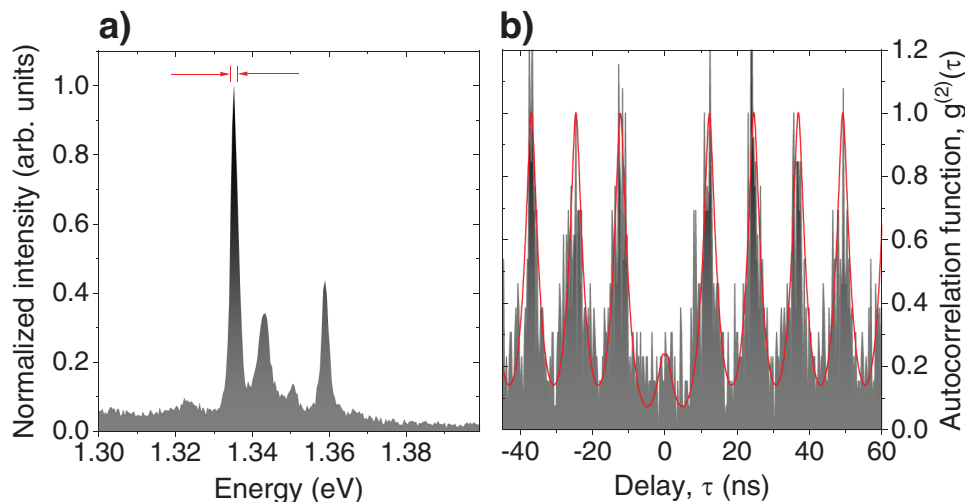TECHNOLOGIES**

www.advquantumtech.com

Figure 4. a) PL spectrum of a QD (labeled QD1) acquired at 10 K and with a CW excitation power of 100 nW. The interval indicated by two red arrows represent the spectral range (2 meV) used for the measurement of the second order autocorrelation function, $g^{(2)}(\tau)$. At the saturation power, with the microsphere on top, and under CW excitation, the photons per second impinging on the first lens are about 0.3×10^6 s^{-1}. b) $g^{(2)}(\tau)$ acquired at $T = 10$ K and with a pulsed excitation power of 400 nW, just below the saturation power, (dark histogram), and its fit (red line) with the model described in the text. It is clear that the $g^{(2)}(0) < 0.5$, confirming the single photon emitter nature of this QD.

of the nitrogen atom number are expected to be Poissonian, the expected standard deviation of x is $\sigma_x = \sqrt{xM/(\rho V N_A)}$ where ρ is the mass density of the material, M is the molar mass, and N_A is the Avogadro constant. Considering a typical QD volume of about 600 nm^3, we obtain $0.0093 < x < 0.0111$, which gives a variation of the GaAs$_{1-x}$N$_x$ bandgap[30] of about ± 7 meV. Therefore, at least at the leading order, the minimum QD inhomogeneous broadening corresponds to a FWHM of about 16 meV.

In order to test the ability of these QDs to emit single photons, we measured their second-order autocorrelation function, $g^{(2)}(\tau)$. In **Figure 4**a we report the CW PL spectrum of a QD (labeled QD1), while in Figure 4b we display the $g^{(2)}(\tau)$ relative to the exciton (X) emission line of the same QD, under pulsed excitation regime. It is to be noted that, in order to improve the signal to noise ratio, a relatively high power (400 nW, about 90% of the saturation power in pulsed excitation regime) was employed for these measurements (micro-PL spectra could be acquired for excitation powers as low as 10 nW). Even though this certainly worsens the single-photon purity, the raw value of $g^{(2)}(\tau)$ at zero delay ($\tau = 0$) is about 0.25, much lower than 0.5, showing the single-photon emitter nature of the QD.

The $g^{(2)}(\tau)$ was fitted with a curve (reported as a solid red line in Figure 4b) based on the solution of a system of rate equations, developed by taking into account the main processes leading to the capture, relaxation, and recombination of carriers in and out of the QD (for a detailed description of the model see ref. [32]). It comprises also a term describing an uncorrelated background. The fit yields a carrier capture time $\tau_{cap} \approx 0.3$ ns, for both electron and hole, and a recombination time $\tau_{rec} \approx 1.84$ ns, in agreement with $\tau_{rec} \approx 2$ ns obtained through time-resolved PL measurements (see Supporting Information). The resulting value of the uncorrelated background results to be about $\approx 20\%$ of the measured coincidences, consistent with the broad emission overlapping with the QD line under consideration. Finally,

the value of $g^{(2)}(0)$, obtained by the fit and due only to the QD line without the uncorrelated background, is less than 0.1.

Once the measure of $g^{(2)}(0)$ for a QD is available, it is also possible to correct the number of emitted photons per second by the factor $\sqrt{1 - g^2(0)}$ in order to eliminate the counts originated from multiple photon emissions.[36] For example, the QD1 generates, in pulsed excitation regime at saturation power, 0.6×10^6 photons s^{-1} impinging on the first lens. Correcting for the factor above, we obtain 0.34×10^6 single-photons s^{-1}. By dividing this number for the laser repetition rate (82 MHz), we obtain that QD1, when coupled with a microsphere, sends toward the collection optics 1 single photon every 240 laser pulses (0.4% of the total). Several factors contribute to keep this value lower than the theoretical one (see **Figure 5**a): the detection efficiency of 4% is an upper limit estimate; the probability of having multi-photon emission from the QD (see above) has been considered; theoretical predictions are highly responsive to small variations of the model; and especially, many other non-radiative, as well as radiative (e.g., the free-exciton recombination from bulk GaAs, other excitonic species in the QD), recombination channels are present in our system, and therefore not every laser pulse results in the emission of a single photon from the QD.

After demonstrating the possibility to "laser write" GaAs$_{1-x}$N$_x$ QDs, we verified another "optical advantage" that the presence of the microspheres brings to the table, that is, the collection enhancement.

The best way to compare different approaches used to outcouple the radiation from an emitter is to give the percentage of the radiation extracted into the air and the shape of the emission pattern. Simply giving the percentage of collected luminescence is useful to set a world record but not to properly give the information about the potentiality of a technology, without considering the fact that some papers report the percentage of collected luminescence with respect to that extracted into the air, not with respect to the total emitted. The collection
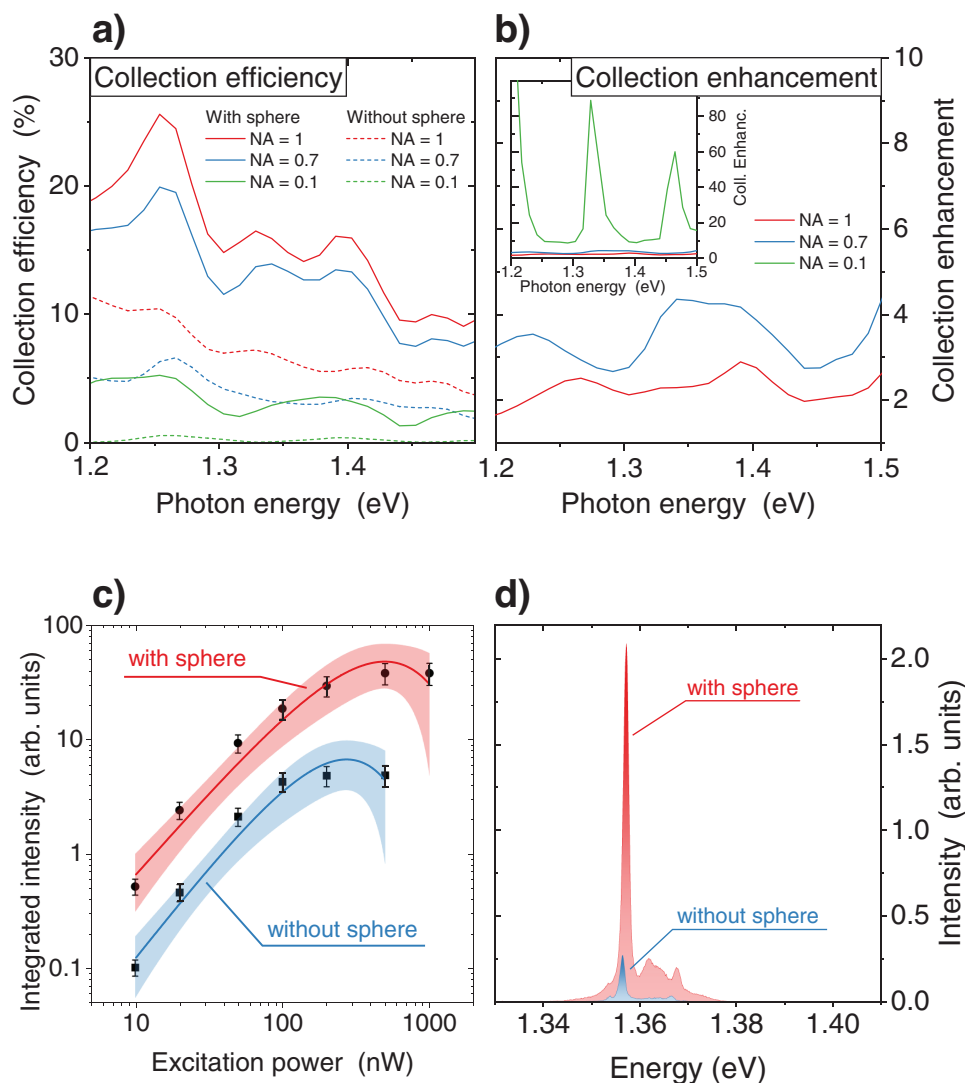
**ADVANCED
SCIENCE NEWS**

www.advancedsciencenews.com

**ADVANCED
QUANTUM
TECHNOLOGIES**

www.advquantumtech.com

Figure 5. a,b) FDTD simulations of the luminescence collection efficiency and luminescence collection enhancement associated with the presence of a dielectric microsphere for different NAs. The inset in (b) has a different scale on the vertical axis in order to show the NA = 0.1 curve. c) Integrated intensity at 10 K of the main transition (X) of a QD (labeled QD2) with a sphere on top (circles) and after sphere removal (squares), as a function of the excitation power. At the saturation power, with the microsphere on top, and under CW excitation, the photons per second impinging on the first lens are about 4×10^6 s^{-1}. The solid lines are the best fits with Equation (S1), Supporting Information, (the filled areas represent the 95% confidence bands). The CW spectra at $P = 500$ nW are reported in panel (d) for comparison. It is worth noting that, as shown in panel (b), the predicted collection enhancement for NA = 0.7 at 1.357 eV is 4.3 while the experimental value obtained from the ratio of the intensities of the two fitting curves at their saturation power is 7.3. The difference is attributed to sensitivity of the simulation results to the initial conditions (see main text).

enhancement, instead, is a useful number to compare technologies consisting in objects that can be inserted between the collection optics and the emitting objects (SILs, microspheres). It is defined as the ratio between the collected power with the microsphere over the collected power without the microsphere.

Using FDTD simulations, both the collection efficiency and the collection enhancement were estimated for several values of NA. We considered a dipole buried 33 nm below the surface of the sample (a value corresponding to the center of the QW in our sample) and with the polarization axis parallel to the sample surface. Our QDs can be approximated as cylinders with diameter larger than their height, which implies a larger probability of having the exciton transition dipole moment parallel to the sam-

ple surface.[37] This condition gives higher collection efficiencies, as well as a higher collection enhancement (simulations not shown). The simulations were performed considering the geometry and the optical constants of our sample (see Figure 2). The results of our simulations as it concerns the estimated collection efficiency and enhancement are shown in Figure 5a,b. As shown in Figure 5a, the percentage of collected power, even without the microsphere, is higher with respect to the simple case of semi-infinite substrate (2%). This is easily explained by the small thickness of the membrane with respect to the wavelength and by the back reflection due to the GaAs/air interface. The collection enhancement due to the presence of the microsphere is reported in Figure 5b and it is the result of the combination of three different

**ADVANCED
SCIENCE NEWS**
www.advancedsciencenews.com

**ADVANCED
QUANTUM
TECHNOLOGIES**
www.advquantumtech.com

physical phenomena:[23] Purcell enhancement (≈ 1, negligible in our case); reduction of light lost by total internal refraction due to near-field coupling between the GaAs and the microsphere (red curve); higher directionality of the emission. The Purcell factor and the near field coupling are NA-independent and their combined effect can be observed looking at the NA = 1 curve. The increase in the directionality of the emission is clearly observed for small NAs, for NA = 0.1, in particular, resonances are observed.

In order to experimentally measure the collection enhancement, first we measured a QD (labeled QD2) with a sphere on top, and then after removing the sphere. The sphere was mechanically wiped away by a tapered optical fiber with a tip of about 200 nm (SNOM tip) mounted on translation stages (see Supporting Information for a video of the sphere removal process). Since the presence of the sphere can influence not only the collection but also the excitation power per unit area, PL spectra at 10 K, before and after the sphere removal, were acquired as a function of the excitation power. Indeed, the saturation power corresponds to an identical excitation condition, allowing to compare the intensities. The integrated intensity as a function of the excitation power for a QD with the main peak at 1.357 eV before and after sphere removal is reported in Figure 5c. Fitting Equation (S1) (see Supporting Information) to the data results in the solid lines of Figure 5c. The ratio of the intensities of these two curves at the saturation power gives the collection enhancement, which is equal to 7.3 ± 0.7 (1 standard deviation). The value predicted by FDTD simulations for NA = 0.7 at 1.357 eV (see Figure 5b) is 4.3. The difference between these two values can be attributed to the unstable behavior of the simulations: large differences in the simulation results are obtained even with small changes of the simulation conditions. In this respect, it is important to note that the simulations assume ideal fabrication parameters, which might deviate significantly from the real ones; just to make an example, the assumption of perfect, mirror-like GaAs/air interfaces is clearly unrealistic, especially given that the lower surface was obtained by chemical etching. This could easily result in an overestimate of the collection efficiency of the suspended GaAs membrane in the absence of the microsphere and, thus, in an underestimate of the collection enhancement due to the latter. For the sake of completeness, in Figure 5d we have reported the PL spectra of the QD before and after the sphere removal with an excitation power as close as possible to the saturation power. The enhancement of the collected signal is clearly observed.

Finally, in order to investigate the physical origin of the collection enhancement, which, as explained above, should be mainly due to an improved directionality of the emission, we measured the angular distribution of the emission of a QD (labeled QD3), with a microsphere on top, whose spectrum is reported in **Figure 6**a. The normalized angular emission pattern in k-space is reported in Figure 6c. Analogously, we reported in Figure 6b,d the spectrum and the normalized angular emission pattern in k-space of the GaAs$_{1-x}$N$_x$/GaAs QW before hydrogenation: this measurement was performed to mimic a point-like emission (like a QD) without a microsphere (without the sphere, the detected QD emission was too weak to perform k-resolved measurements; in and by itself, this is a testament to the effectiveness of the microspheres in improving the collection efficiency). It is clear that the angular distribution of the emission without the

microsphere is much broader than that with the microsphere. The effect of the microsphere, as explained above, is to increase the directionality of the emission of the emitters placed below it. This result is more clearly observed looking at the profiles of the angular emission patterns of Figure 6c,d. Cutting these two experimental maps along a direction passing through the center of the emission, and averaging against all possible directions, the profiles reported in Figure 6e are obtained (blue circles and red squares). In order to compare these profiles against the theoretical expectations, we simulated the same system described above and we considered the far field pattern as a function of the emission angle—with and without the presence of the microsphere —obtaining the curves displayed in Figure 6e as solid lines. Comparing the curves, a clear agreement is found.

It is of the utmost relevance to note that an in-plane misalignment of the QDs with the point contact of the sphere on the sample surface would result in an angular shift of the emission of the order of 0.059 ° nm^{-1} (or, equivalently, the photonic jet is shifted by 17 nm per degree when the incident beam is tilted; see Supporting Information). Using the estimated precision in determining the central point in k space ($\sigma_k/(2\pi/\lambda) = 0.02$) and the estimated precision in determining the center of the emission ($\sigma_k/(2\pi/\lambda) = 0.02$), we can therefore estimate that the QD-sphere alignment is, at 1 standard deviation, ± 30 nm, highlighting the power of our approach. Analogously, it would be possible to fabricate sphere-misaligned QDs via tilted illumination, obtaining a deterministic beam steering of the quantum emitters.

4. Conclusions

In conclusion, in this work we have demonstrated the possibility to create GaAs$_{1-x}$N$_x$ QDs exploiting, for the first time, photonic jets to locally tune the hydrogen content in dilute nitrides. This fabrication method inherently ensures a near-perfect (± 30 nm) spatial alignment between the QD and the microsphere used to generate the photonic jet, thus leading to the maximization of the broadband enhancement of the collection efficiency ($\times 7.3$) for the light emitted by the QD. This technique has other several advantages: the fabrication is performed at room temperature, in air and without any lithography or etching procedure; it is low-cost with respect to most QD fabrication techniques; the emission can be tuned over a range larger than 200 meV controlling the hydrogen removal; it is, in principle, possible to cover both telecommunication wavelength windows by tuning the nitrogen concentration and/or by introducing indium in GaAs$_{1-x}$N$_x$; the QDs are rewritable, since the fabricated nanostructures can be erased and rewritten multiple times, simply by re-hydrogenating the sample and by repeating the fabrication process.

Our approach can be compared to other "geometric" approaches, like SILs and microlenses. In order to have a fair comparison between SIL, microlenses, and microspheres, we considered a semi-infinite substrate in which the emitters are buried. SILs are bulky and very sensitive to the air gap between them and the sample. Their maximum collection enhancement is about n_L^2 [20] and does not depend strongly on the objective NA. Microlenses, micrometer-sized SILs directly carved by nanolithography on top of the emitters, do not have the bulky nature drawback and the air-gap problem of the SIL.
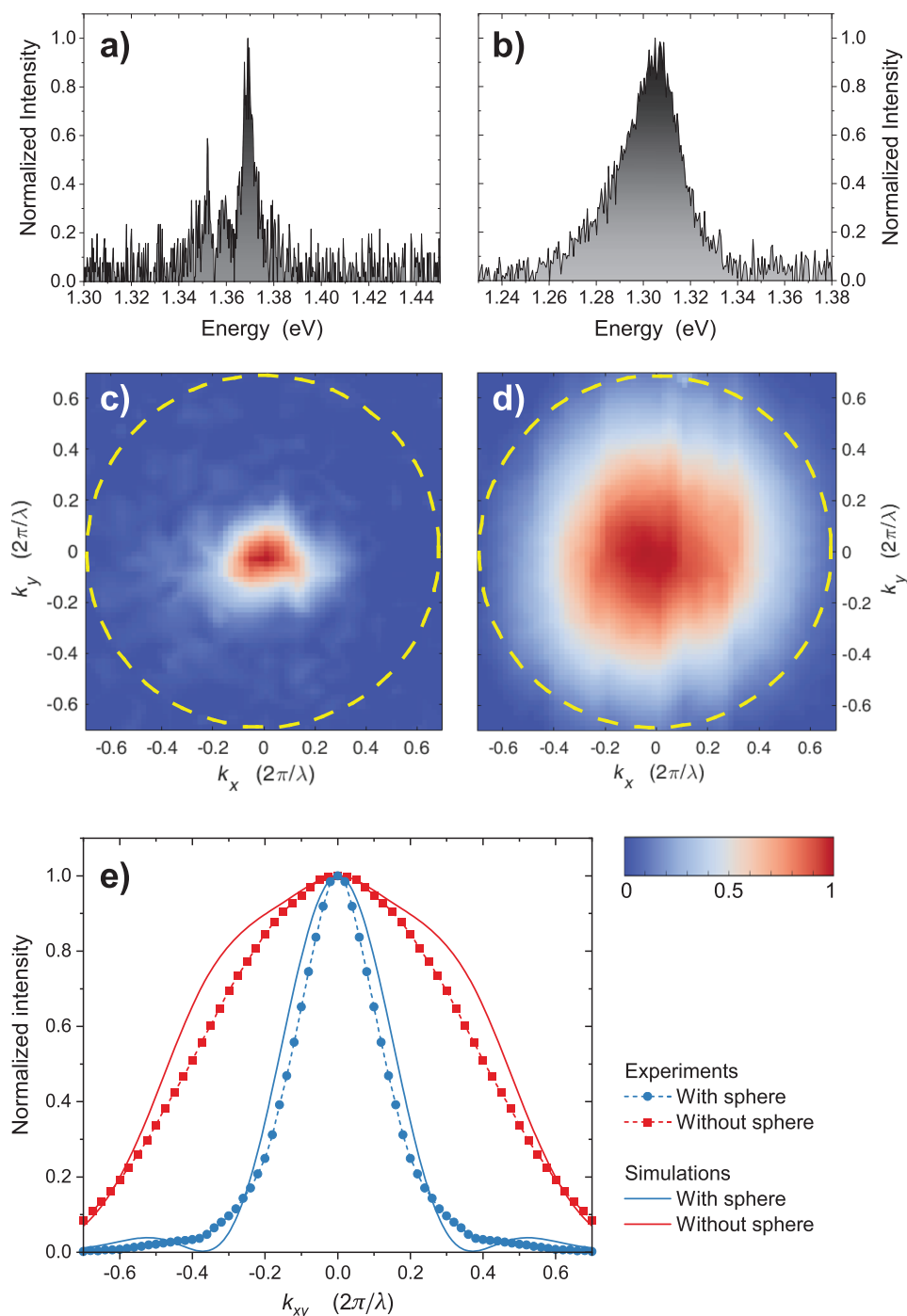
**ADVANCED
SCIENCE NEWS**

www.advancedsciencenews.com

**ADVANCED
QUANTUM
TECHNOLOGIES**

www.advquantumtech.com

Figure 6. a,b) PL spectra of a QD (labeled QD3) under CW excitation, with a microsphere, and of the GaAsN/GaAs QW before hydrogenation, without a microsphere, respectively. These spectra correspond to the center of the maps reported in (c,d), respectively. c) PL angular emission map of the emission of the QD3 with a microsphere on top ($T = 10$ K, $P_{exc} = 300$ nW, energy interval 1.362–1.376 eV). The yellow dashed circle represents the NA (NA = 0.7) of the objective used. d) PL angular emission map of the QW signal without a microsphere on top ($T = 10$ K, $P_{exc} = 400$ μW, energy interval 1.290–1.317 eV). The yellow dashed circle represents the NA (NA = 0.7) of the objective used. This measurement was performed to mimic a point-like emission without a microsphere. e) Experimental angular profiles (blue circles and red squares) extracted from the maps in panel (c,d), respectively, by a proper radial average. These data are compared with FDTD simulated angular profiles (blue and red solid lines) of emitters (emitting at 1.37 and 1.305 eV) with and without a microsphere, respectively, buried in a material with 3.5 refractive index, 33 nm below the surface.

**ADVANCED
SCIENCE NEWS**

www.advancedsciencenews.com

**ADVANCED
QUANTUM
TECHNOLOGIES**

www.advquantumtech.com

Their drawbacks are mainly related to the nanofabrication, and especially to the difficulty of carving them exactly aligned to a pre-existing QD. Their maximum collection enhancement is about n_L^2, even though, for particular geometries of the microlens and for low NA objectives, slightly larger collection efficiencies can be reached.[14] For glass ($n_L = 1.5$) microspheres, on the other hand, the collection enhancement consistently exceeds n_L^2. For large NA objectives ($0.5 < NA < 0.7$) the enhancement ranges between 6 and 10 in the wavelength range of interest ($\lambda \approx 900$ nm, see Figure S5h, Supporting Information), that is, it is comparable to what can be achieved with high-n SILs and microlenses. For small NAs (e.g., 0.1), on the other hand, microspheres allow reaching collection enhancement values as high as 40, much larger than those reachable with other approaches.

Despite the several advantages, there are some issues, such as the large homogeneous broadening of the emission (≈ 1 meV), the limited brightness, and the lack of control over the microspheres deposition. In our opinion, these problems can be potentially solved in a straightforward manner: as far as the large QD linewidth is concerned, the broadening is likely linked to surface defects,[38] and can thus be reduced by growing a thicker capping layer on top of the $GaAs_{1-x}N_x$:H/GaAs QW (from the simulations we observe that the photonic jet keeps a narrow waist for nearly 1 µm when propagating in GaAs). Moreover, this would contribute also to an enhancement in the QD brightness, especially if combined with a QW of higher quality and an efficient back-reflector (e.g., a distributed Bragg reflector). Regarding the possibility to obtain site-controlled QDs, the microsphere positioning can be forced by engineering the material's surface prior to deposition.[39]

A last remark about the possibility to reach the so called GHz regime, widely regarded as one of the ultimate goals of deterministic single-photon sources.[40] Considering the typical exciton radiative lifetime of our QDs at low temperature (0.5–3 ns) (see Supporting Information), we could easily reach the 100 MHz regime. The GHz regime could be within reach only by lowering the exciton radiative lifetime. The fabrication of a PhC cavity in the membrane before sphere deposition could greatly decrease the radiative lifetime, thanks to the Purcell effect. This is one of the reasons why we suspended the QW by removing the sacrificial layer. A discussion of the effects of the integration of single site-controlled GaAsN QDs in a PhC cavity on the radiative lifetime can be found in ref. [32]. Within this context, the method we developed to remove individual microspheres from the sample (see Supporting Information) could be further refined to precisely move and align the microspheres with the center of the PhC cavity. In this configuration, the presence of the microsphere should greatly enhance light extraction from the cavity, which is known to be an issue for high-quality factor PhC structures.[41] Other approaches for reducing the radiative lifetime are also possible.[40]

This work also paves the way for several possible developments: from the realization of complex structures such as QDs arrays, by packing up the microspheres in a honeycomb structure,[42] to the development of innovative approaches to the creation of site-controlled QDs, by controlling the microspheres deposition or by mounting a microsphere at the end of an optical fiber (which, in turn, could be mounted on a nanopositioner).

5. Experimental Section

Sample preparation: A $GaAs_{1-x}N_x$/GaAs ($x = 0.011$) quantum well (QW) was grown by molecular beam epitaxy with the following structure: a GaAs buffer (130 nm) was deposited on a (001) GaAs substrate, followed by a sacrificial layer of $Al_{0.7}Ga_{0.3}As$ (1500 nm), a GaAs lower cladding (130 nm), a $GaAs_{0.989}N_{0.011}$ layer (6 nm), and a GaAs upper cladding (30 nm).[43] The sample was then moved to a vacuum chamber, where it was kept at a constant temperature of 190 °C and exposed to a flux of hydrogen ions generated by a low energy Kaufman source (beam energy 100 eV, beam size about 3 cm) with an ion current density of 25 µA cm^{-2} for about 500 s. The total dose of H was 8×10^{16} ions cm^{-2}, sufficient for a complete passivation of the nitrogen atoms. An excess of hydrogen had the only effect to favor the formation of N-2H-H complexes with respect to the N-2H ones, thus introducing a moderate compressive strain in the sample.[29,44]

Membrane Preparation: The sacrificial layer between the QW and the substrate was removed to obtain an array of well-separated circular suspended membranes with a diameter of few micrometers.[45] In order to achieve this goal, an array of annular apertures of 4 µm in diameter and 200 nm in width was patterned by electron beam lithography (Vistec EPBG 5HR working at 100 kV) into a positive-tone resist (ZEP 520 A) spun on the sample's surface and developed in a mixture of MIBK:IPA (1:1). Then, the apertures were transferred into the sample, down to the (Al,Ga)As layer, by means of a chlorine-based reactive ion etching (with a Cl$_2$:BCl$_3$:Ar gas mixture). Finally, the residual masking resist was removed with anisole, and the GaAs membranes were released by a wet etching in HF (5%) of the (Al,Ga)As sacrificial layer.

Microspheres Deposition: The microspheres were composed of silicon dioxide with mean diameter of 2.06 µm and standard deviation of 0.05 µm (Microparticles GmbH). The microspheres come in aqueous suspension making up 5% of the weight/volume percentage. The spheres were deposited with an airbrush (Point Zero PZ-270) with 0.2 mm nozzle diameter. The sample was placed at large distance from the airbrush, in order to ensure the complete evaporation of the liquid contained in the sphere solution, thus leaving only the spheres before hitting the sample. Additionally, a high air pressure was used for the airbrush; as a result, small droplets similar to a mist were formed, which also aids the evaporation process.

QD Fabrication: The QD fabrication was performed by exposing a single microsphere with the 532 nm line of a continuous wave (CW) diode-pumped solid-state laser(CNI MLL-III-532) focused on the sample by a home-made confocal setup equipped with a 10× objective (NA=0.2). The laser beam was ideally placed in the microsphere's center, and each exposure lasted for a few seconds. The exposure time was controlled by an automatic shutter (ThorLabs SH05 connected to a controller KSC101) which granted a temporal reproducibility of about 0.2%. The sample was aligned using a Physik Instrument x–y translational stage and the sample surface was observed with a CMOS camera, connected to the confocal setup by a 50:50 beamsplitter. The uncertainty in positioning was around 250 nm. The QDs creation process was done in air and at room temperature.

PL Characterization: The optical properties of the fabricated nanostructures were studied by micro-photoluminescence (micro-PL). The sample was kept at 10 K in a low-vibration Janis ST-500 continuous He-flow cryostat, which in turn was mounted on a Physik Instrumente x–y translation stage for scanning the sample surface. The luminescence was collected by a home-made confocal microscope setup equipped with an infinity corrected Mitutoyo 100× objective (378-806-3, NA = 0.7). The luminescence was spectrally dispersed using an Acton SP2300i spectrograph, mounting a 600 gr/mm grating and a 1200 gr/mm grating (blazed at 1000 nm and 750 nm, respectively), and detected using a Si CCD Acton Pixis 100F. The spatial resolution of the system is about 700 nm, while the spectral resolution is about 400 µeV using the 600 gr/mm grating and 250 µeV using the 1200 gr/mm grating. The detection efficiency of the setup is reported in the Supporting Information.

For time-integrated measurements the excitation source was a CW diode-pumped solid-state laser at 532 nm (CNI MLL-III-532). Time-resolved PL (TR-PL) measurements were performed using the time

correlated single photon counting (TCSPC) technique. The excitation source was provided by a mode-locked Ti:Sapphire tunable laser (Spectra Physics Tsunami, 700-900 nm spectral range, 200 fs pulse duration, 12.2 ns pulse period) frequency doubled by a BBO crystal and pumped by a frequency doubled CW Nd-YAG laser. The spectrally dispersed luminescence was selected using the exit slit of the spectrograph and sent to a PerkinElmer SPCM-AQR-16 single photon counting APD. For second-order autocorrelation ($g^{(2)}(\tau)$) measurements, a Hanbury Brown and Twiss intensity interferometer was used. The luminescence was split by a 50:50 non-polarizing beam splitter and each beam was dispersed by an Acton SP2300i spectrograph. A PerkinElmer SPCM-AQR-16 single photon counting APD was present at the exit slit of each spectrograph. Both for the TR-PL and $g^{(2)}(\tau)$ measurements the APD signals were processed with proper fast electronics (Tennelec TAC, Canberra MCA) interfaced with a computer. The time resolution of TCSPC and $g^{(2)}(\tau)$ measurements is about 400 ps, entirely due to the APD rise-time jitter (the TAC jitter is about 20 ps).

The angle-resolved PL measurements were obtained using a pinhole, mounted on two programmable stages, inserted along the collection path.

Supporting Information

Supporting Information is available from the Wiley Online Library or from the author.

Acknowledgements

Conflict of Interest

The authors declare no conflict of interest.

Author Contributions

G.P. performed the lithographic patterning of QW and the membrane release. M.F. performed the hydrogenation of the QW, carried out the modeling of second order autocorrelation histograms, and made the sketches in Figure 1. T.H. and H.M. carried out the microsphere deposition, SEM micrographs, and FDTD simulations of Figure 5. F.B. and A.R. carried out the QD fabrication, all the experimental measurements (partly with D.T. collaboration) and analysis, with input from M.G., G.P., M.F., and S.S. A.R. carried out FDTD simulations of Figures 2 and 6 with input from F.B. and M.G. The manuscript was written by F.B. and A.R. with the help of M.F. and all the other authors.

Data Availability Statement

The data that support the plots within this paper and other findings of this study are available from the corresponding author upon reasonable request.

Keywords

collection enhancement, dilute nitrides, microspheres, photonic jets, site-controlled quantum dots

[1] M. A. Nielsen, I. L. Chuang, *Quantum Computation and Quantum Information*, Cambridge University Press, Cambridge **2010**.

[2] *Single Semiconductor Quantum Dots* (Ed: P. Michler), Springer, Berlin **2009**.

[3] *Handbook of Nanophysics* (Ed: K. D. Sattler), CRC Press, Boca Raton, FL **2011**.

[4] S. G. Lukishova, L. J. Bissell, *Quantum Photonics: Pioneering Advances and Emerging Applications*, Springer Series in Optical Sciences, Vol. *217*, Springer, Berlin **2019**, pp. 103–178.

[5] P. Kok, W. J. Munro, K. Nemoto, T. C. Ralph, J. P. Dowling, G. J. Milburn, *Rev. Mod. Phys.* **2007**, *79*, 135.

[6] S. Hepp, M. Jetter, S. L. Portalupi, P. Michler, *Adv. Quantum Technol.* **2019**, *2*, 1900020.

[7] O. Gazzano, S. Michaelis de Vasconcellos, C. Arnold, A. Nowak, E. Galopin, I. Sagnes, L. Lanco, A. Lemaître, P. Senellart, *Nat. Commun.* **2012**, *4*, 1425.

[8] K. H. Madsen, S. Ates, A. Javadi, S. M. Albrecht, I. Yeo, S. Stobbe, P. Lodahl, *Phys. Rev. B* **2014**, *90*, 155303.

[9] F. Liu, A. J. Brash, J. O'Hara, L. M. P. P. Martins, C. L. Phillips, R. J. Coles, B. Royall, E. Clarke, C. Bentham, N. Prtljaga, I. E. Itskevich, L. R. Wilson, M. S. Skolnick, A. M. Fox, *Nat. Nanotechnol.* **2018**, *13*, 835.

[10] L. Sapienza, M. Davanço, A. Badolato, K. Srinivasan, *Nat. Commun.* **2015**, *6*, 7833.

[11] D. Gérard, A. Devilez, H. Aouani, B. Stout, N. Bonod, J. Wenger, E. Popov, H. Rigneault, *J. Opt. Soc. Am. B* **2009**, *26*, 1473.

[12] M. Gschrey, A. Thoma, P. Schnauber, M. Seifried, R. Schmidt, B. Wohlfeil, L. Krüger, J. H. Schulze, T. Heindel, S. Burger, F. Schmidt, A. Strittmatter, S. Rodt, S. Reitzenstein, *Nat. Commun.* **2015**, *6*, 7662.

[13] M. Sartison, S. L. Portalupi, T. Gissibl, M. Jetter, H. Giessen, P. Michler, *Sci. Rep.* **2017**, *7*, 39916.

[14] M. Sartison, L. Engel, S. Kolatschek, F. Olbrich, C. Nawrath, S. Hepp, M. Jetter, P. Michler, S. L. Portalupi, *Appl. Phys. Lett.* **2018**, *113*, 032103.

[15] J. Claudon, J. Bleuse, N. S. Malik, M. Bazin, P. Jaffrennou, N. Gregersen, C. Sauvan, P. Lalanne, J. M. Gérard, *Nat. Photonics* **2010**, *4*, 174.

[16] O. J. Trojak, S. I. Park, J. D. Song, L. Sapienza, *Appl. Phys. Lett.* **2017**, *111*, 021109.

[17] O. J. Trojak, C. Woodhead, S.-I. Park, J. D. Song, R. J. Young, L. Sapienza, *Appl. Phys. Lett.* **2018**, *112*, 221102.

[18] P. Stepanov, A. Delga, N. Gregersen, E. Peinke, M. Munsch, J. Teissier, J. Mørk, M. Richard, J. Bleuse, J. M. Gérard, J. Claudon, *Appl. Phys. Lett.* **2015**, *107*, 141106.

[19] K. A. Serrels, E. Ramsay, P. A. Dalagarno, B. Gerardot, J. A. O'Connor, R. H. Hadfield, J. Warburton, D. T. Reid, *J. Nanophotonics* **2008**, *2*, 021854.

[20] S. Moehl, H. Zhao, B. Dal Don, S. Watcher, H. Kalt, *J. Appl. Phys.* **2003**, *93*, 6265.

[21] Y. Chen, M. Zopf, R. Keil, F. Ding, O. G. Schmidt, *Nat. Commun.* **2018**, *9*, 2994.

[22] D. G. Gérard, J. Wenger, A. Devilez, D. Gachet, B. Stout, N. Bonod, E. Popov, H. Rigneault, *J. Opt. Soc. Am.* **2008**, *16*, 15297.

[23] F. Biccari, T. Hamilton, A. Ristori, S. Sanguinetti, S. Bietti, M. Gurioli, H. Mohseni, *Part. Part. Syst. Charact.* **2019**, *37*, 1900431.

[24] W. Wu, A. Katsnelson, O. G. Memis, H. Mohseni, *Nanotechnology* **2007**, *18*, 485302.

[25] P. Ferrand, J. Wenger, A. Devilez, M. Pianta, B. Stout, N. Bonod, E. Popov, H. Rigneault, *Opt. Express* **2008**, *16*, 6930.

**ADVANCED
SCIENCE NEWS**

www.advancedsciencenews.com

**ADVANCED
QUANTUM
TECHNOLOGIES**

www.advquantumtech.com

[26] A. Heifetz, S. C. Kong, A. V. Sahakian, A. Taflove, V. Backman, *J. Comput. Theor. Nanosci.* **2009**, *6*, 1979.

[27] A. Bonakdar, M. Rezaei, R. L. Brown, V. Fathipour, E. Dexheimer, S. J. Jang, H. Mohseni, *Optics Lett.* **2015**, *40*, 2537.

[28] L. Chen, Y. Zhou, Y. Li, M. Hong, *Appl. Phys. Rev.* **2019**, *6*, 021304.

[29] *Hydrogenated Dilute Nitride Semiconductors* (Ed: G. Ciatto), Jenny Stanford Publishing, Singapore **2015**.

[30] U. Katsuhiro, S. Ikuo, H. Tatsuo, A. Tomoyuki, N. Takayoshi, *Appl. Phys. Lett.* **2000**, *76*, 1285.

[31] R. Trotta, A. Polimeni, M. Capizzi, *Adv. Funct. Mater.* **2012**, *22*, 1782.

[32] M. Felici, G. Pettinari, F. Biccari, A. Boschetti, S. Younis, S. Birindelli, M. Gurioli, A. Vinattieri, A. Gerardino, L. Businaro, M. Hopkinson, S. Rubini, M. Capizzi, A. Polimeni, *Phys. Rev. B* **2020**, *101*, 205403.

[33] G. Pettinari, M. Felici, F. Biccari, M. Capizzi, A. Polimeni, *Photonics* **2018**, *5*, 10.

[34] F. Biccari, A. Boschetti, G. Pettinari, F. La China, M. Gurioli, F. Intonti, A. Vinattieri, M. S. Sharma, M. Capizzi, A. Gerardino, L. Businaro, M. Hopkinson, A. Polimeni, M. Felici, *Adv. Mater.* **2018**, *30*, 1705450.

[35] N. Balakrishnan, G. Pettinari, O. Makarovsky, L. Turyanska, M. W. Fay, M. D. Luca, A. Polimeni, M. Capizzi, F. Martelli, S. Rubini, A. Patanè, *Phys. Rev. B* **2012**, *86*, 155307.

[36] M. Pelton, C. Santori, J. Vučković, B. Zhang, G. S. Solomon, J. Plant, Y. Yamamoto, *Phys. Rev. Lett.* **2002**, *89*, 233602.

[37] A. Mohan, P. Gallo, M. Felici, B. Dwir, A. Rudra, J. Faist, E. Kapon, *Appl. Phys. Lett.* **2011**, *98*, 253102.

[38] N. Ha, T. Mano, Y.-L. Chou, Y.-N. Wu, S.-J. Cheng, J. Bocquel, P. M. Koenraad, A. Ohtake, Y. Sakuma, K. Sakoda, T. Kuroda, *Phys. Rev. B* **2015**, *92*, 075306.

[39] J. Hou, M. Li, Y. Song, *Angew. Chem., Int. Ed.* **2018**, *57*, 2544.

[40] A. Schlehahn, R. Schmidt, C. Hopfmann, J.-H. Schulze, A. Strittmatter, T. Heindel, L. Gantz, E. R. Schmidgall, D. Gershoni, S. Reitzenstein, *Appl. Phys. Lett.* **2016**, *108*, 021104.

[41] M. Toishi, D. Englund, A. Faraon, J. Vučković, *Optics Express* **2009**, *17*, 14618.

[42] J.-Y. Choi, T. L. Alford, C. B. Honsberg, *Langmuir* **2014**, *30*, 5732.

[43] J. M. Ulloa, P. M. Koenraad, M. Hopkinson, *Appl. Phys. Lett.* **2008**, *93*, 083103.

[44] L. Wen, M. Stavola, W. B. Fowler, R. Trotta, A. Polimeni, M. Capizzi, G. Bisognin, M. Berti, S. Rubini, F. Martelli, *Phys. Rev. B* **2012**, *86*, 085206.

[45] G. Pettinari, A. Gerardino, L. Businaro, A. Polimeni, M. Capizzi, M. Hopkinson, S. Rubini, F. Biccari, F. Intonti, A. Vinattieri, M. Gurioli, M. Felici, *Microelectron. Eng.* **2017**, *174*, 16.

2100045 (11 of 11)

Supporting Information

Photonic jet writing of quantum dots self-aligned to dielectric antennas

A. Ristori, T. Hamilton, D. Toliopoulos, M. Felici, G. Pettinari, S. Sanguinetti,
M. Gurioli, H. Mohseni, F. Biccari*

*Corresponding author: francesco.biccari@unifi.it

1.   Effect of a nanometric air gap on photonic jet formation

The microspheres were deposited on the sample using an airspray (see Experimental Section in the manuscript) which should guarantee perfect adhesion between the spheres and the substrate. However, in order to verify the formation of a photonic jet even in a non-contact situation, we have performed a FDTD simulation with and without a thin layer of vacuum between the sphere and the sample (Fig. S1). The simulations show that an air gap of 5 nm does not give rise to any relevant modification of the electric field distribution and therefore to the photonic jet.
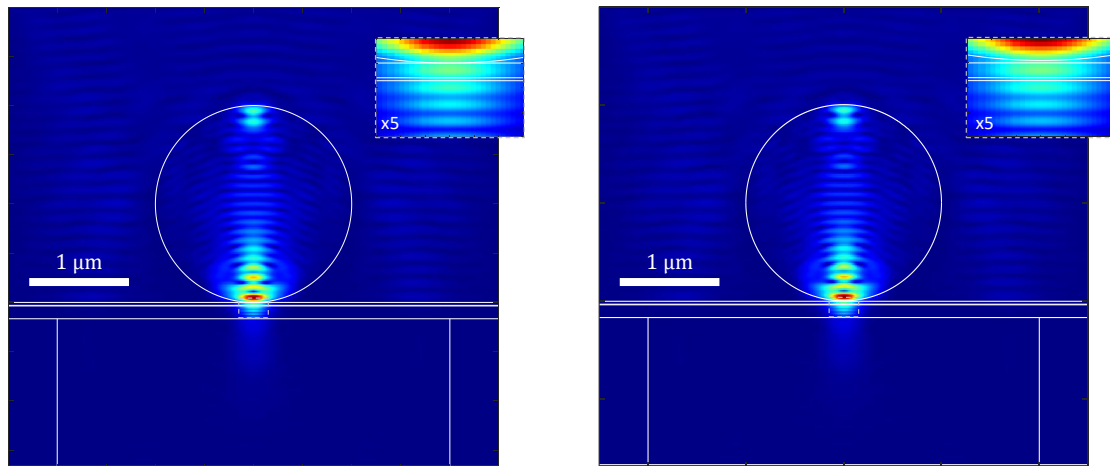

Figure S1: a) Poynting vector magnitude obtained by FDTD simulation of our sample with one microsphere on top of a suspended GaAs$_{1-x}$N$_x$:H/GaAs QW, under illumination with a plane wave (λ = 532 nm). The white lines represent the contour of our sample and the microsphere. The inset shows a x5 magnification of the photonic jet area. b) Poynting vector magnitude obtained by FDTD simulation of our sample in the same condition of a) but with a thin layer of 5 nm of vacuum between the microsphere and the QW.

2. Identification of the QD emission lines

In order to identify the origin of the different transitions visible in the PL spectra of each QD, we studied the evolution of their integrated intensity as a function of the CW excitation power. Indeed, according to a Poissonian model for the level occupation probability[1], the integrated intensity, I_{PL}, of the exciton (X) and biexciton (XX) PL lines follow different filling dynamics, described by:

$$I_{PL} = C \left(a P^b \right)^n e^{-a P^b} \tag{S1}$$

where $n = 1$ for X and $n = 2$ for XX, P is the excitation power, and a, b and C are three constants. The average number of excitons present in the QD at a given power, $\langle n \rangle$, is
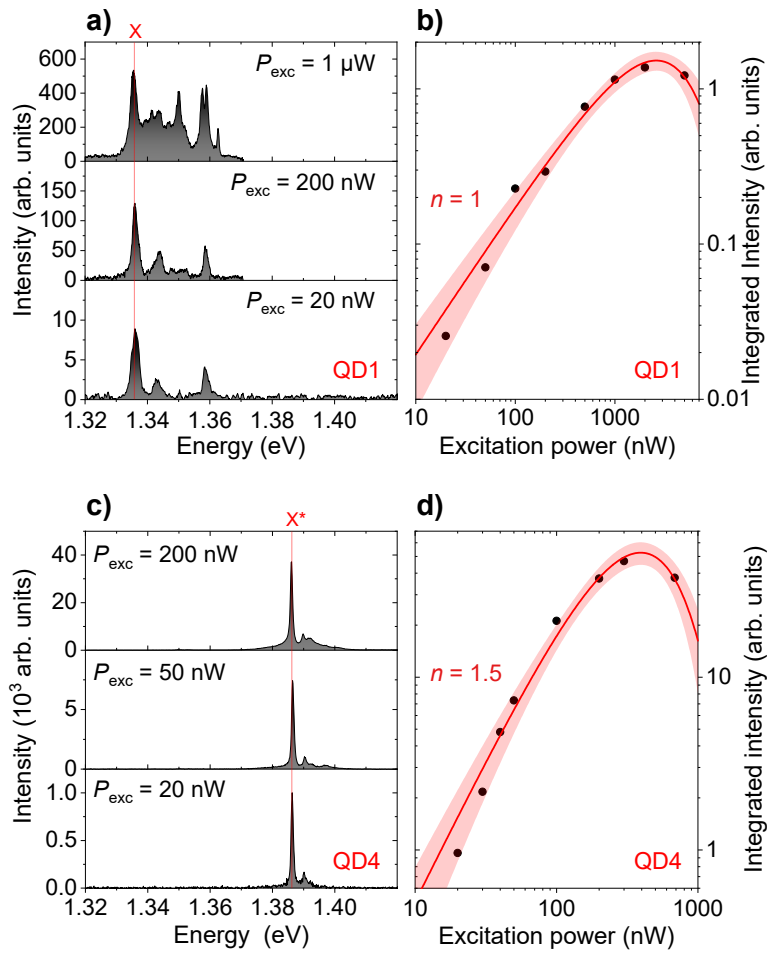

Figure S2: a) and c) display selected PL spectra acquired at $10\,\mathrm{K}$ on two different QDs, labeled QD1 and QD4, at different CW excitation powers. b) and d) show the integrated intensity of the main transition of the two QDs, highlighted with a semitransparent red line in panels a) and c), as a function of the excitation power. Eq. (S1) is used to fit the experimental data (black dots), yielding the red lines shown in the figure (the filled areas represent the 95% confidence bands). These fits allow us to identify the main transitions of QD1 and QD2 as an exciton (X, $n = 1$) and as a trion (X*, $n = 1.5$), respectively.

given by aP^b. It has been proved experimentally [1] that Eq. (S1) can also describe the behaviour of a charged exciton (X*), provided that $n = 1.5$.

Fig. S2 summarizes the power dependence of the PL spectra of two QDs, whose main emissions are at 1.336 eV (QD1) and at 1.386 eV (QD2), respectively. Three selected spectra are reported for each QD in Figs. S2a and S2c, whereas Figs. S2b and S2d include the integrated intensity of the main peak as a function of the excitation power (black dots) and the fits (red lines) obtained with Eq. (S1). The parameter n is fixed before the fitting procedure, it can assume only the value 1, 1.5, 2 and it is chosen in order to obtain b as close as possible to 1.

The results of the fit show that the main QD1 peak can be associated with an exciton (X), and the QD2 peak with a charged exciton (X*). The fitting parameters for the two QDs are: $n = 1$, $a = (5.1 \pm 1.9) \times 10^{-4}$ nW^{-b}, $b = (0.96 \pm 0.05)$, and $n = 1.5$, $a = (2.0 \pm 0.6) \times 10^{-3}$ nW^{-b}, $b = (1.11 \pm 0.05)$, respectively. As expected, the X* has a narrower linewidth, ≈ 900 μeV, than the X, ≈ 2 meV, due to the higher tolerance of charged excitonic species for the electric field fluctuations generated by charging and discharging of surrounding defects [2].

The saturation power under CW excitation multiplied by the ratio between the exciton lifetime and the laser repetition rate (which is, for example, about 2 for QD1) gives an estimate of the saturation power under pulsed excitation regime.

3.   Estimation of the capture volume of the QDs

From the nature (n) and saturation power (P_s) of the emissions, the capture volume (V_c) of the QDs, a good proxy for their quality, can be estimated. $\langle n \rangle = V_c G \tau$, where G is the e-h pair generation term and τ is the e-h pairs lifetime, which in our case is about 1 ns. Moreover, Eq. 1 of the manuscript reaches saturation at $\langle n \rangle = n$, thus $V_c = n/(G_s \tau)$.

Considering the GaAs absorption coefficient at 532 nm, $\alpha = 7 \times 10^4$ cm^{-1}, a spot area $A = 1$ μm^2 (with NA = 0.7 the photonic jet is very broad[3]), and the photon energy at $E_{ph} = 2.33$ eV (corresponding to a wavelength of 532 nm), we can estimate $G_s = \alpha P_s/(A E_{ph})$. Using $P_s = 2689$ nW and $P_s = 389$ nW for QD1 and QD4, respectively (obtained considering that at saturation $\langle n \rangle = a P_s^b = n$), we finally obtain $V_c = 30 \times 10^3$ nm^3 and $V_c = 205 \times 10^3$ nm^3 for QD1 and QD4, respectively.

Assuming a cylindrical geometry for the QDs, with a height $L = 6$ nm and a diameter $2R = 10$ nm and $2R = 7$ nm for QD1 and QD4, respectively, we can estimate the capture length, L_c, considered constant all around the nanostructure. We find $L_c = 14$ nm and $L_c = 32$ nm for QD1 and QD4, respectively, values similar to (or larger than) the QD size, indicating the good quality of the material. In particular, the larger value obtained for QD4 indicates its better quality with respect to QD1, probably due to a different environment with smaller defects concentration, which explains also the different linewidths of the emissions.

3

4. Time-resolved PL measurements

We have performed time-resolved micro-PL measurements on the emissions of our QDs. Fig. S3 shows the time-resolved PL measurement of the QD (labeled as QD1) emission used for the second order autocorrelation function ($g^{(2)}$) measurement reported in Fig. 4b of the Main Manuscript. The fits (red line) were performed with a single (Fig. S3a) and a double (Fig. S3b) exponential, respectively, convoluted with a Gaussian. The Gaussian curve models the impulse response function of our system (FWHM = 400 ps).

The double exponential perfectly fits the data, consistent with other cases reported in the literature for GaAsN QDs (see, e.g. Ref. [4], although for the sake of completeness we must mention that a second QD, correctly described by a single exponential, is also reported in that work). The time constants of the double exponential obtained from the fit are: $\tau_1 = (3.08 \pm 0.06)$ ns and $\tau_2 = (0.67 \pm 0.03)$ ns.

The single exponential provides an average time constant, which can be directly compared with the time constant obtained from the $g^{(2)}$ fit reported in Fig. 4b of the Main Manuscript. Indeed, the model used to fit the $g^{(2)}$ data also describes the decay of the QD just by a single exponential (τ_{rec}). Indeed, adding another free parameter to the $g^{(2)}$ model would clearly give an overfitting of the curve, considering the noise present in the autocorrelation data.

The time constant of the single exponential results in a value of $\tau = (2.00 \pm 0.05)$ ns. This is in good agreement with the value of $\tau_{rec} = 1.84$ ns found by the fit of the $g^{(2)}$ measurement reported in Fig. 4b of the Main Manuscript.
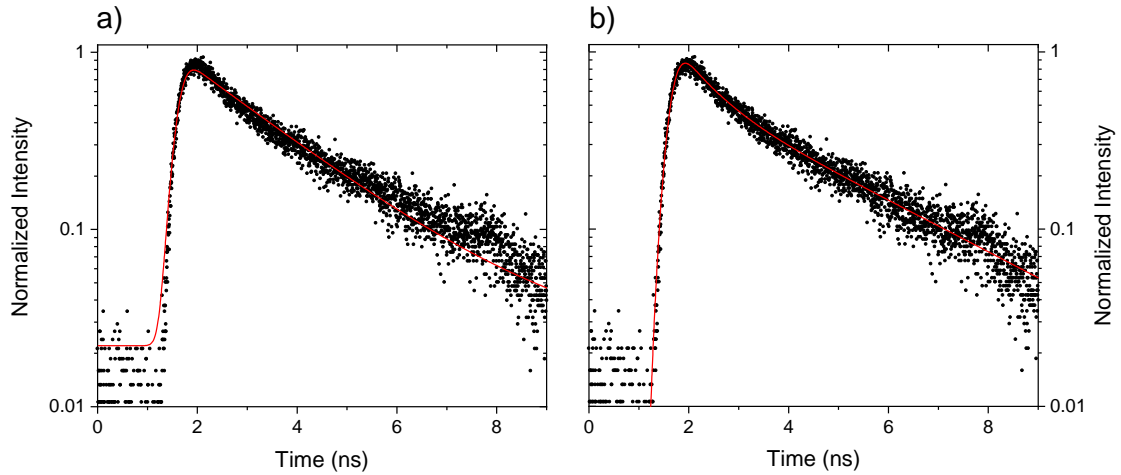

Figure S3: Time-resolved micro-PL measurements of the QD excitonic emission (black dots) and its fit (red curve). a) Fit performed with a single exponential convoluted with a Gaussian (system impulse response). The fit gives a value of the exponential time constant of $\tau = (2.00 \pm 0.05)$ ns. b) Fit performed with a double exponential convoluted with a Gaussian (system impulse response). The fit gives the values of the exponential time constants of $\tau_1 = (3.08 \pm 0.06)$ ns and $\tau_2 = (0.67 \pm 0.03)$ ns.

5.   Removal of the microspheres

The microspheres deposited on the sample surface can be mechanically removed by a tapered optical fiber with a tip having the diameter of about 200 nm (SNOM tip) mounted on translation stages. A video (`sphere-removal.mp4`, H264 video codec, no audio) showing the removal of a single sphere on top of a sample membrane is available as Supporting material.

6.   Angular shift

The photonic jet produced by illuminating a microsphere can be rigidly shifted by tilting the incident plane wave. This was verified through several FDTD simulations, which are shown in Fig. S4. In order to quantify this effect, we estimated the jet center position as a function of the incident angle, finding a constant shift of 17 nm/°.

Analogously, the reverse condition, the tilt of the beam originating from a QD at different distances from the sphere contact point, must give the same value of 17 nm/°, by
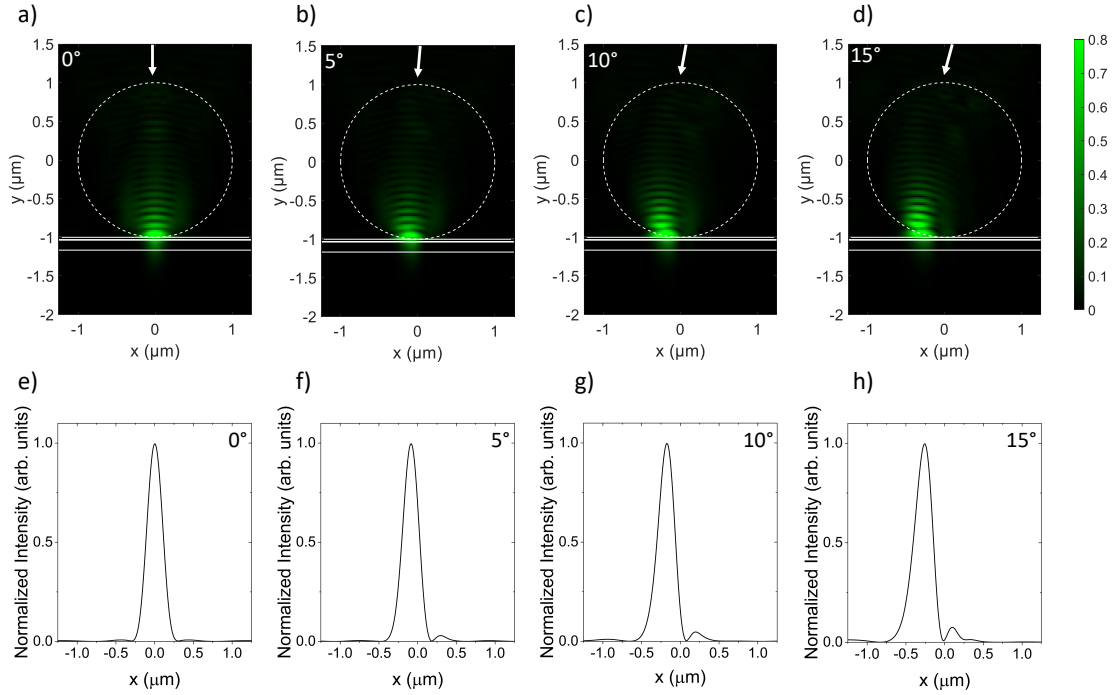

Figure S4: a), b), c) and d) display FDTD simulations of a series of photonic jets. They are obtained illuminating a dielectric microsphere with a plane wave ($\lambda = 532$ nm) at different incident angles, indicated by an arrow. The angle is measured clockwise with respect to the normal to the plane and its value is indicated on top of each panel. The white solid lines represent the contour of the sample while the dashed line represents the microsphere. e), f), g) and h) show the profiles of the photonic jets obtained within the QW for the incident angle displayed in a), b), c), d), respectively. Analyzing the peak position as a function of the wave incident angle, we obtain a shift of 17 nm/°.

Helmholtz reciprocity principle. The simulations and a simple analytical model are given in the Supporting Information of Ref. [3], where, for small angle, the relation between the QD off-axis distance (d) and the emerging beam angle (θ) is given by $d = r\theta$, r being the microsphere radius. If θ is expressed in degrees (°) and considering $r = 1000$ nm, we obtain $d = (17.45 \, \text{nm}/°) \, \theta$.

7. Collection enhancement as a function of the objective's NA

We have performed FDTD simulations of the luminescence collection enhancement associated with the presence of a dielectric microsphere for a series of different numerical apertures (NAs) and considering a semi-infinite GaAs substrate. Fig. S5 displays the results, combined with the simulated behaviour of the collection enhancement for a QD emission line at 1.357 eV as a function of the NA of the collecting optics.
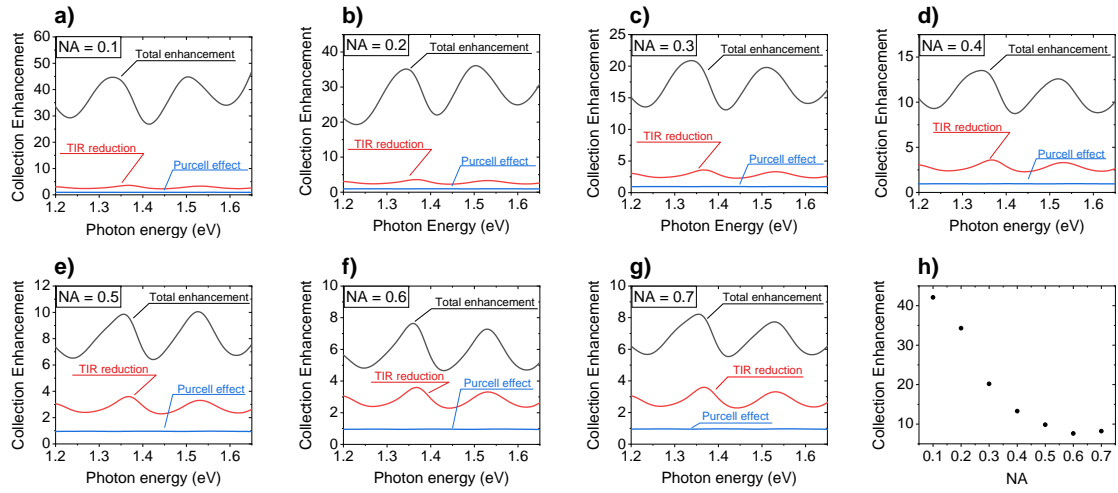

Figure S5: a-g) FDTD simulations of the luminescence collection enhancement associated with the presence of a dielectric microsphere for different NAs. In all the graph the blue curve represents the enhancement due to Purcell effect, the red one the enhancement due to the reduction of the light lost by total internal refraction (TIR), and the black curve represents the total collection enhancement. h) Luminescence collection enhancement as a function of the NA for a QD emission line at 1.357 eV.

8. Estimation of the PL setup efficiency

An upper estimate of the overall efficiency of our system is given by the product of the tabulated data (see Tab. 1) for all the elements of our setup, which yields a value of about 4% at 930 nm.

Table 1: Tabulated efficiencies of all the components of our PL setup.

Object	Efficiency at 930 nm
Cryostat JANIS ST-500 uncoated quartz window	0.93
Objective Mitutoyo 378-806-3	0.35
Mirror Thorlabs PF10-03-P01P (×3)	$0.97 \times 0.97 \times 0.97$
Dichroic mirror Semrock FF560-FDi01-25x36	0.98
Focusing lens Thorlabs AC127-019-B-ML	0.99
Grating Princeton Instr. 600 gr/mm, BLZ 1 μm	0.80
Silver mirrors inside spectrograph SP2300i (×3)	$0.97 \times 0.97 \times 0.97$
CCD Princeton Instr. PIXIS 100F (1340×100)	0.19
TOTAL SETUP	**0.040**

References

[1] M. Abbarchi, C. Mastrandrea, T. Kuroda, T. Mano, A. Vinattieri, K. Sakoda, M. Gurioli. *J. Appl. Phys.*, **106**, 053504 (2009). `doi:10.1063/1.3197848`.

[2] M. Abbarchi, C. Mastrandrea, T. Kuroda, T. Mano, A. Vinattieri, T. Mano, N. Koguchi, K. Sakoda, M. Gurioli. *Phys. Status Solidi C*, **6**, 886 (2009). `doi:10.1002/pssc.200880653`.

[3] F. Biccari, T. Hamilton, A. Ristori, S. Sanguinetti, S. Bietti, M. Gurioli, H. Mohseni. *Part. Part. Syst. Charact.*, **37**, 1900431 (2019). `doi:10.1002/ppsc.201900431`.

[4] S. Birindelli, M. Felici, J. S. Wildmann, A. Polimeni, M. Capizzi, A. Gerardino, S. Rubini, F. Martelli, A. Rastelli, R. Trotta. *Nano Lett.*, **14**, 1275 (2014). `doi:10.1021/nl404196y`.